Science Bulletin xxx (xxxx) xxx

Contents lists available at ScienceDirect

Science Bulletin

journal homepage: www.elsevier.com/locate/scib

Short Communication

Thickness-dependent topological phases and flat bands in rhombohedral multilayer graphene

Hanbo Xiao [a,1], Cheng Chen [a,b,1], Xin Sui [c,1], Shihao Zhang [d,1], Mengzhao Sun [a], Han Gao [a], Qi Jiang [a], Qiao Li [a,b], Lexian Yang [e], Mao Ye [f], Fangyuan Zhu [f], Meixiao Wang [a], Jianpeng Liu [a,b], Zhibin Zhang [c], Zhujun Wang [a], Yulin Chen [a,b,g], Kaihui Liu [c,h,*], Zhongkai Liu [a,b,*]

[a] School of Physical Science and Technology, ShanghaiTech University, Shanghai 201210, China
[b] Laboratory for Topological Physics, ShanghaiTech University, Shanghai 201210, China
[c] State Key Laboratory for Mesoscopic Physics, Frontiers Science Centre for Nano-optoelectronics, School of Physics, Peking University, Beijing 100871, China
[d] School of Physics and Electronics, Hunan University, Changsha 410082, China
[e] State Key Laboratory of Low Dimensional Quantum Physics, Department of Physics, Tsinghua University, Beijing 100084, China
[f] Shanghai Synchrotron Radiation Facility, Shanghai Advanced Research Institute, Chinese Academy of Sciences, Shanghai 201210, China
[g] Department of Physics, Clarendon Laboratory, University of Oxford, Oxford, OX1 3PU, UK
[h] Interdisciplinary Institute of Light-Element Quantum Materials and Research Centre for Light-Element Advanced Materials, Peking University, Beijing 100871, China

ARTICLE INFO

Article history:
Received 10 January 2025
Received in revised form 16 January 2025
Accepted 17 January 2025
Available online xxxx

Rhombohedral multilayer graphene (RMG) has recently been demonstrated to be an exceptional research platform hosting a wide range of quantum phenomena. These include superconductivity [1], various symmetry-broken states (spin, valley, and layer) [2], integer and fractional quantum anomalous Hall effect [3], and Chen insulator states [4]. A key factor in tuning the properties of RMG is the number of layers, as different quantum phases have been observed only in samples with specific layer counts. For example, the fractional Chern insulator phase has been observed exclusively in a 5-layer sample [5], the quantum anomalous Hall in a 4-layer sample [3], and superconductivity in a 3-layer sample [1].

The intriguing properties of RMG and its layer-tuning capabilities arise from its unique electronic structure, characterized by flat surface bands. The formation of these flat bands can be described by the 3D generalization of the Su-Schrieffer-Heeger (SSH) model [6], which explains the 2*N*-2 gapped bulk subbands and the surface flat bands (SFBs). The SFBs correspond to edge states in the SSH model, making RMG a 3D generalization of the 1D topological insulator (TI) described by the SSH model. As *N* increases, both the SFBs and subbands can be continuously tuned, with the number of subbands and crossing points in the SFB increasing accordingly. In the $N = \infty$ limit (rhombohedral graphite), the system is predicted to transition into a topological Dirac nodal spiral semimetal (DNSS), where the gapped subbands merge into a 3D Dirac cone that spirals with opposite helicity around the K and K′ points, and the SFB evolves into the drumhead surface state [7].

The intriguing evolution of the band structure and topological properties with varying *N* highlights the need for a comprehensive investigation of the electronic structure of RMG. To date, several angle-resolved photoemission spectroscopy (ARPES) studies have reported the electronic structure of RMG films [8], but these studies have been limited in resolution and scope. A systematic investigation of the layer-dependent evolution of the electronic structure, particularly as *N* approaches the ∞ limit, remains elusive. Such studies are crucial for understanding the interplay between strong electron correlations, topological phase transitions, and the emergence of exotic quantum states in this system.

In this work, we systematically explored the electronic structure of RMG using synchrotron-based spatially resolved ARPES (NanoARPES) measurements for N = 3, 24, and the bulk limit ($N \sim 50$). Our observations reveal the topological electronic structures predicted by the SSH model, including the SFBs and the gapped subbands. As *N* increases, the topological flat bands persist, while the number of subbands originating from the bulk states increases, the subband energy spacing reduces, and the subband gap closes. For rhombohedral graphite ($N \sim 50$), the gapped subbands transition into gapless 3D Dirac cones that spiral around the K and K′

* Corresponding authors.
E-mail addresses: khliu@pku.edu.cn (K. Liu), liuzhk@shanghaitech.edu.cn (Z. Liu).
[1] These authors contributed equally to this work.

https://doi.org/10.1016/j.scib.2025.01.036
2095-9273/

points in momentum space. Simultaneously, the SFBs evolve into drumhead surface states with numerous crossing points, establishing a topological DNSS system. The observed band evolution aligns well with density function theory (DFT) calculations, confirming the thickness-dependent topological phases in RMG. These findings establish RMG as a unique topological flat-band system for investigating strong correlations and topological physics.

RMG is a graphene allotrope with ABC stacking (Fig. 1a), where each atom connects to the nearest neighbor in an adjacent layer, either directly above or below it. RMG can be conceptually mapped onto a 1D SSH chain and is topologically nontrivial, hosting SFBs at the top and bottom layers (Fig. 1a). It can therefore be described as the 3D generalization of the SSH model. More realistically, its electronic structure is explained by the Slonzewski-Weiss-McClure model [9]. The total Berry phase in the K valley is $N\pi$, where N represents the number of layers, illustrating the nontrivial topological nature of the SFBs [10] (details can be found in Supplementary material (SM) Text S1). As N increases, the number of SFB crossing points increases, and the gaps between the subbands gradually close. In the bulk limit, a topological phase transition occurs, resulting in the formation of DNSS, where all subbands merge into gapless Dirac cones [7].

Our NanoARPES measurements on N = 3, 24 and 48 RMG confirm the predicted band structure evolution, as shown in the high-symmetry cuts across the K and K′ points (Fig. 1c–e). The observed band structures for N = 3 RMG show a strong contrast to those in Bernal-stacked trilayer (ABA) graphene (See Fig. S3 online). The measured subband gap, estimated from the energy spacing between E_F and the top of the hole-type subbands, is approximately 276 meV. The SFB has a bandwidth exceeding 107 meV, estimated from E_F to the band bottom, as detailed in the zoomed-in cut in Fig. 1c(ii).

In the N = 24 sample (nominal thickness, though the actual number of layers may be smaller due to potential stacking faults; see Fig. S4 online) (Fig. 1d), the SFB and the gapped hole-type subbands remain observable. Interestingly, the number of subbands increases, while the subband gap reduces to 83 meV. The SFB bandwidth is over 60 meV, estimated from E_F to the band bottom. We also note the development of k_z dispersion (Fig. S5 online), similar to observations in other multilayer graphene systems.

Finally, in the bulk rhombohedral graphite sample (N = 48) (Fig. 1e), the large number of subbands merge into the bulk continuum, reducing the subband gap to zero and forming a Dirac cone structure. The SFBs evolve into a flat band situated at the Dirac nodes at E_F. The measured bandwidth of the SFB is greater than 45 meV, as shown in Fig. 1e(iii). The dispersion measured in the bulk sample agrees well with the calculated results (we used N = 48 to simulate the bulk situation; see Fig. 1e(iv)). The band parameters for different N values are summarized in Table S1 (online), and additional ARPES data showing the momentum extension of the flat band are presented in Fig. S6 (online).

To further investigate the topological DNSS state in the bulk limit, we conducted detailed ARPES measurements on the bulk RMG sample, with result presented in Fig. 2. For large N, the gapless Dirac cones form a distinctive nodal spiral around the K and K′ points in the Brillouin zone (BZ) of RMG (Fig. 2a). The bulk-boundary correspondence of the nodal spiral protects the existence of drumhead surface states, which evolve from the SFBs [11]. From the measured photoemission spectra at various photon energies (Fig. 2b), we observe that the band dispersion consists of two components. The first component is the bulk Dirac cones, which exhibit significant variations. This evolution is characterized by a counterclockwise rotation of the Dirac node spiral, moving from the right side to the left side (see schematic on top of Fig. 2b; see further discussion below). The measured dispersions are well captured by DFT calculations at different k_z values (bottom row of Fig. 2b), confirming the bulk nature of these bands. Despite the rapid changes in bulk bands, the flat bands near E_F are consistently observed at different photon energies (Fig. 2c). These flat bands are absent in the DFT calculations for bulk rhombohedral graphite but appear in the large-N slab calculation (shaded regions in the bottom row of Fig. 2b), confirming their surface nature. As the observed surface flat bands are surrounded by the Dirac nodal spiral structure, they form the so-called drumhead surface state. The coexistence of the nodal spiral structure and the drumhead surface state confirms the topological DNSS nature of rhombohedral graphite (see also theoretical model in Text S1 online).

According to the Slonzewski-Weiss-McClure model, for large N, the band crossings are continuously arranged along a helical spiral, forming the Dirac nodal spiral [7]. The helicity of the Dirac node spiral is opposite at the K and K′ points due to time-reversal symmetry. This unique feature can be observed by measuring the Fermi surface (FS) at different k_z values using various photon energies [12]. From the FS maps probed at the K (Fig. 2e) and K′ points (Fig. 2f) with different photon energies, we trace the evolution of surface states and the Dirac nodes by following the strongest spectral intensity. The observed Dirac nodes are situated on a circle with the same momentum radius (indicated by the dashed curves

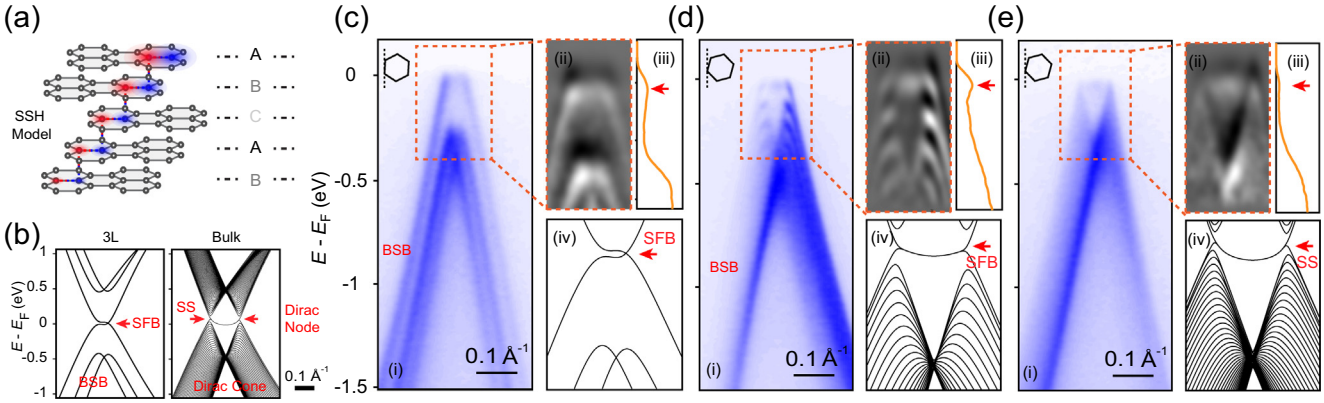

Fig. 1. Tuning the electronic structure RMG with the layer number N. (a) Structure of RMG. Red and blue atoms form the 1D SSH chain, and the colored clouds represent the wavefunction amplitude localized on each atom in the SSH chain. (b) DFT-calculated band structure along the Γ-K-M direction for N = 3 and 100. (c) (i) Plot of the band dispersion of N = 3 RMG along the direction labeled in the inset. (ii) Zoom-in plot of the second derivative of the photoemission intensity near the SFB. (iii) Plot of the energy distribution curve at the K/K′ point, with the SFB marked by red arrow. (iv) DFT-calculated band structure for N = 3 RMG. (d) Same as (c) but for N = 24 RMG. (e) Same as (c) but for N = 48 RMG. SFB: surface flat bands. BSB: bulk subbands. SS: surface state.

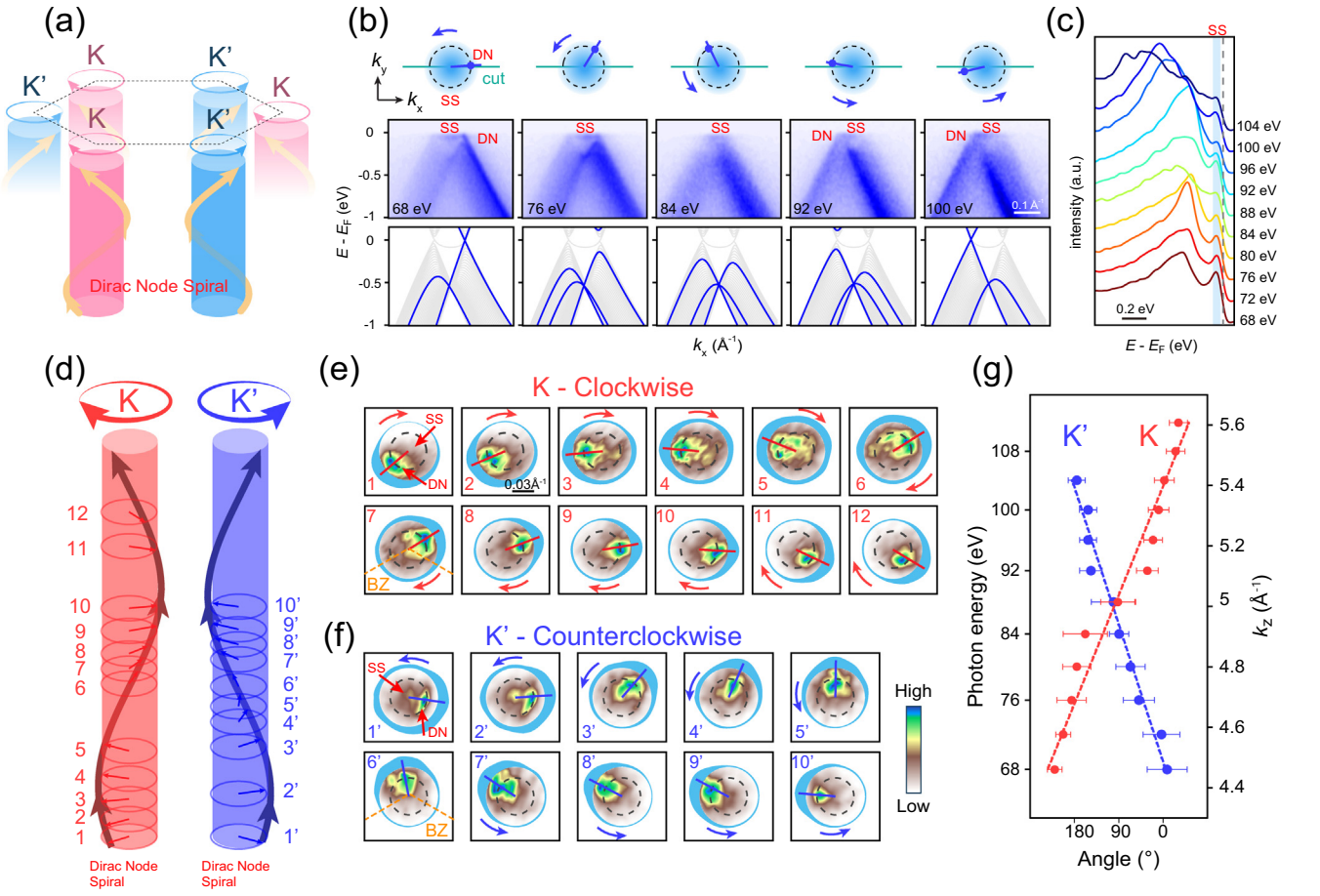

Fig. 2. Drumhead surface states and Dirac nodal spirals in rhombohedral graphite. (a) Schematic of the Dirac node spiral and drumhead surface states in rhombohedral graphite. (b) (Upper) Band dispersion cut across the K′ point measured at various photon energies. (Lower) DFT-calculated dispersion of rhombohedral graphite along the same direction, corresponding to different k_z values. The shaded regions show the slab calculation results for N = 48 RMG. (c) Stacked plot of the energy distribution curves along the K′ point at different photon energies, with the bandwidths of the surface states highlighted by shaded regions. (d) Schematic of the momentum-space Dirac node spiral at the K and K′ points. The shaded column represents the drumhead surface states, and the numbered circles indicate the measured Fermi surface (FS) at each photon energy. Arrows denote the extracted angles of the Dirac nodes, as shown in (e) and (f). (e) FS at the K point measured at various photon energies, as labelled in (d). The dashed circle represents the projection of the spiral, and the angular intensity distribution curves are shown as blue shades around each map. Red lines indicate the extracted angles of the FS intensity along the dashed circle. (f) Same as (e), but near the K′ point. (g) Extracted angle of the FS intensity around the K/K′ points versus photon energy, plotted alongside the linear fit of the helicity. The data were collected at 20 K using linearly polarized photons with horizontal polarization. SS: surface state. DN: Dirac node.

in Fig. 2e, f). These nodes rotate clockwise/counterclockwise around K and K′, respectively, as k_z increases, forming a spiral structure in momentum space (see schematic in Fig. 2d, where the arrow indicates the position of the Dirac node for each k_z). The angular positions of the measured Dirac nodes are plotted as a function of photon energy and k_z values in Fig. 2g. These observations are consistent with theoretical predictions (see Text S1 online), thereby confirming the DNSS nature of bulk rhombohedral graphite.

While the qualitative evolution of the subband gap and energy spacing with N is consistent with DFT calculations, the flatness of the SFBs is tunable by the layer number N, highlighting its critical role in the formation of unique quantum transport phenomena in RMG. An appropriate level of electron correlation may create a so-called "sweet spot" with optimal band flatness, facilitating the observation of multiple quantum phases [13]. The strong correlation effects are evident in the SFBs near E_F, as demonstrated by various experimental and theoretical work [3]. Increased band flatness in large-N RMG could further enhance electron instabilities, paving the way for interaction-driven correlated quantum states. Additionally, the 3D flat band in bulk RMG embodies the 3D quantum geometry of Bloch wave functions, which results in large superfluid stiffness in all three spatial directions [14]. Thus, RMG serves as a unique platform for studying the interplay between topology and correlation.

In conclusion, our observations reveal the characteristic SFBs and gapped subband electronic structures of RMG, along with their layer-dependent evolutions. These findings demonstrate a unique thickness-driven topological phase transition from a 3D generalization of the SSH model to a topological DNSS. Our measurements of the SFBs and nodal spiral structures provide a cornerstone for further investigations into the electronic structure of RMG and its relation with nontrivial quantum phases.

After submitting this manuscript, we noted the publication of a similar ARPES study addressing the topological phase of rhombohedral graphite [15].

Conflict of interest

The authors declare that they have no conflict of interest.

Acknowledgments

We acknowledge the support from the National Natural Science Foundation of China (92365204, 12274298, 52025023, 12304217), the National Key R&D Program of China (2022YFA1604400/03,

2022YFA1403500/04), the Strategic Priority Research Program of Chinese Academy of Sciences (XDB33000000), Fundamental Research Funds for the Central Universities from China, and the New Cornerstone Science Foundation through the XPLORER PRIZE.

Author contributions

Kaihui Liu and Zhongkai Liu designed and supervised the project. Hanbo Xiao and Cheng Chen conducted the ARPES experiments and analyzed the data, with assistance from Han Gao, Qi Jiang, Mao Ye, Fangyuan Zhu, and Meixiao Wang. Xin Sui and Zhibin Zhang prepared the RMG devices. Shihao Zhang and Jianpeng Liu performed the band structure calculations. Mengzhao Sun and Zhujun Wang carried out the EM experiments. Qiao Li, Lexian Yang, and Yulin Chen provided technical and conceptual assistance. All authors contributed to the writing of the manuscript.

Appendix A. Supplementary material

Supplementary material to this article can be found online at https://doi.org/10.1016/j.scib.2025.01.036.

References

[1] Zhou H, Xie T, Taniguchi T, et al. Superconductivity in rhombohedral trilayer graphene. Nature 2021;598:434–8.
[2] Liu K, Zheng J, Sha Y, et al. Spontaneous broken-symmetry insulator and metals in tetralayer rhombohedral graphene. Nat Nanotechnol 2024;19:188–95.
[3] Han T, Lu Z, Yao Y, et al. Large quantum anomalous Hall effect in spin-orbit proximitized rhombohedral graphene. Science 2024;384:647–51.
[4] Sha Y, Zheng J, Liu K, et al. Observation of a chern insulator in crystalline ABCA-tetralayer graphene with spin-orbit coupling. Science 2024;384:414–9.
[5] Lu Z, Han T, Yao Y, et al. Fractional quantum anomalous hall effect in multilayer graphene. Nature 2024;626:759–64.
[6] Min H, MacDonald AH. Electronic structure of multilayer graphene. Prog Theor Phys 2008;176:227–52.
[7] Ho C-H, Chang C-P, Lin M-F. Evolution and dimensional crossover from the bulk subbands in ABC-stacked graphene to a three-dimensional Dirac cone structure in rhombohedral graphite. Phys Rev B 2016;93:075437.
[8] Bao C, Yao W, Wang E, et al. Stacking-dependent electronic structure of trilayer graphene resolved by nanospot angle-resolved photoemission spectroscopy. Nano Lett 2017;17:1564–8.
[9] McClure JW. Band structure of graphite and de Haas-van alphen effect. Phys Rev 1957;108:612–8.
[10] Koshino M, McCann E. Trigonal warping and Berry's phase N π in ABC-stacked multilayer graphene. Phys Rev B 2009;80:165409.
[11] Xiao R, Tasnádi F, Koepernik K, et al. Density functional investigation of rhombohedral stacks of graphene: topological surface states, nonlinear dielectric response, and bulk limit. Phys Rev B 2011;84:165404.
[12] Sobota JA, He Y, Shen Z-X. Angle-resolved photoemission studies of quantum materials. Rev Mod Phys 2021;93:025006.
[13] Cao Y. Rhombohedral graphene goes correlated at four or five layers. Nat Nanotechnol 2024;19:139–40.
[14] Lau A, Hyart T, Autieri C, et al. Designing three-dimensional flat bands in nodal-line semimetals. Phys Rev X 2021;11:031017.
[15] Zhang H, Li Q, Scheer MG, et al. Correlated topological flat bands in rhombohedral graphite. Proc Natl Acad Sci USA 2024;121:e2410714121.